Eur Radiol (2009) 19: 13–23
DOI 10.1007/s00330-008-1122-7

Anno Graser
Thorsten R. C. Johnson
Hersh Chandarana
Michael Macari

Dual energy CT: preliminary observations and potential clinical applications in the abdomen

Received: 12 February 2008
Revised: 7 June 2008
Accepted: 18 June 2008
Published online: 2 August 2008
© European Society of Radiology 2008

A. Graser · T. R. C. Johnson
Department of Clinical Radiology,
University of Munich –
Grosshadern Campus,
Marchioninistr. 15,
81377 Munich, Germany

A. Graser · H. Chandarana · M. Macari
Department of Radiology,
New York University Medical Center,
560 1st Ave,
New York, NY, 10016, USA

A. Graser (✉)
Department of Clinical Radiology,
University of Munich –
Grosshadern Hospitals,
Marchioninistr. 15,
81377 Munich, Germany
e-mail: anno.graser@med.lmu.de

Abstract Dual energy CT (DECT) is a new technique that allows differentiation of materials and tissues based on CT density values derived from two synchronous CT acquisitions at different tube potentials. With the introduction of a new dual source CT system, this technique can now be used routinely in abdominal imaging. Potential clinical applications include evaluation of renal masses, liver lesions, urinary calculi, small bowel, pancreas, and adrenal glands. In CT angiography of abdominal aortic aneurysms, dual energy CT techniques can be used to remove bones from the datasets, and virtual unenhanced images allow differentiation of contrast agent from calcifying thrombus in patients with endovascular stents. This review describes potential applications, practical guidelines, and limitations of dual energy CT in the abdomen.

Keywords Computed tomography · Abdominal imaging · Dual energy CT

Introduction

Technological advances including helical and multi-detector row acquisition as well as dose modulation continuously increase the clinical applications and diagnostic value of CT [1]. A recent development in CT has been the introduction of dual source technology [2]. On such CT systems, two X-ray tubes can be operated at different tube potentials, making "dual energy scanning" possible. Dual energy CT implies simultaneously acquiring data sets at two different photon spectra in a single CT acquisition [3].

There are three main advantages of a dual source CT when compared with a single-source system [2]. First, the tubes can be used in unison at equal tube potentials, permitting increased photon flux in larger patients. Second, since an image can be acquired using 90 degrees of gantry rotation rather than 180, temporal resolution can be increased by a factor of two when using the two tubes at identical kVp levels. Using this technique, a temporal resolution of 83 ms is possible. Third, and most important for abdominal applications, the system can be used such that the tubes operate at different tube potentials. For all applications described in this article, tube currents used were 80 and 140 kVp, as these lead to maximum density differences between different materials and therefore allow for optimum material differentiation [3].

By obtaining CT data at different photon energies, differences in material composition can be detected based on differences in photon absorption. This technique exploits attenuation differences of materials with large atomic numbers like iodine. For example, the attenuation of iodine will be much greater at 80 kVp than at 140 kVp [4]. Importantly, based on the reconstruction of complete 80 kVp and 140 kVp image data sets from the raw data, "virtual unenhanced" and "virtual angiographic" data sets can be generated utilizing various dual energy post-processing

algorithms, which are based on three-material decomposition principles. In the abdomen, the three materials usually analyzed are soft tissue, fat, and iodine [3].

The potential applications of dual energy CT when evaluating the abdomen are numerous. Generation of virtual unenhanced images may obviate the routine need for true unenhanced acquisitions. That is, a single contrast-enhanced acquisition can yield both unenhanced and contrast-enhanced CT data. This is of importance when evaluating the liver, adrenal glands, and kidneys and may be utilized to decrease radiation exposure to patients. Furthermore, differences in attenuation of data acquired at 80 kVp and 140 kVp may be beneficial in the diagnosis of inflammatory and ischemic bowel disease or poorly vascularized tumors such as pancreatic cancer. Finally, the attenuation of vessels is substantially greater when acquired at 80 kVp as opposed to 140 kVp. This may improve vessel detection and evaluation at CT angiography and at the same time allow less iodinated contrast material to be administered. The purpose of this paper is to review our initial experience with the technical aspects, potential clinical applications, as well as current limitations of dual energy CT when evaluating the abdomen and pelvis.

Technical considerations

The first report on dual energy CT was in 1977 [5]. Initial investigations of dual energy were in bone mineral analysis, quantification of hepatic iron and calcium in pulmonary nodules, and for the differentiation of various tissues [5–8]. Despite initial promising results, clinical utilization of dual energy CT was abandoned. At that time two separate consecutive CT data sets needed to be acquired. Neither helical nor MDCT were available, and thus long acquisition times were required, leading to motion misregistration, high image noise due to scattered radiation at low kVp settings, and excessive radiation exposure.

The development of a dual-tube, dual-detector CT system (Somatom Definition, Siemens Medical Solutions, Forchheim, Germany) in 2006 has led to increased investigation and now utilization of dual energy CT. This system consists of two X-ray tubes mounted in one gantry at a 90 degree angle from each other [2]. For each tube, a 64-element detector is present: the "A" detector, which is equal in size to a standard detector (50 cm) used in a single-source 64-slice system, and the "B" detector, which also has a 64-slice design, but with a reduced field of view of 27 cm (see Fig. 1) [2]. This detector array provides high spatial resolution of isotropic 0.38-mm edge-length voxels and allows a rapid acquisition of a large Z-axis volume.

The two X-ray tubes of the CT system can be operated at identical tube potentials to provide an increase in temporal resolution for cardiac examinations [9] or photon flux in obese patients [3]. Alternatively, they can be operated at two different tube energies potentially allowing differentiation various tissues based on different photon absorption rates at high and low kVp settings [3].

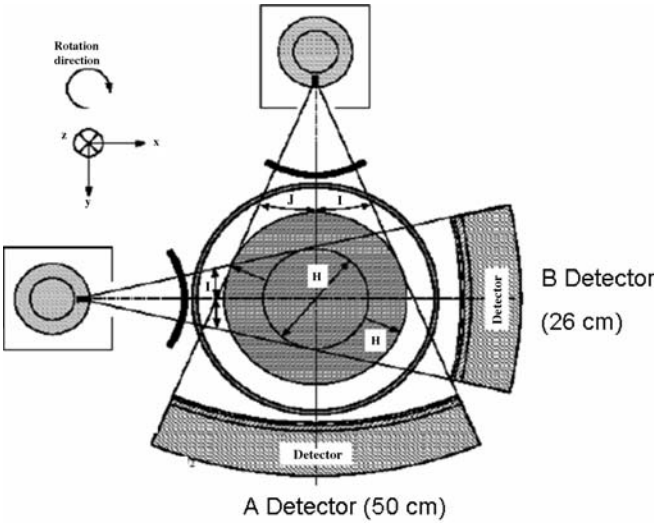

Fig. 1 Technical drawing of the dual source dual-detector CT system. Detector "A" with standard 50 cm FOV and detector "B" with reduced 26 cm FOV are mounted in the gantry at a 90° angle. (Modified from [2] with permission)

A limitation of dual energy CT in the abdomen and pelvis is that the smaller size of the B detector (27 cm) will prevent imaging of the entire FOV in larger patients. Therefore, patients may have to be positioned off center if the location of the lesion is known and it is in the periphery of the FOV (see dual energy imaging of renal masses). It is important to position the table with the patient in the center of the field of view in the x (right/left) as well as in the y (anterior/posterior) axis. Therefore, it is mandatory to acquire both a.p. and lateral topograms to make sure that the table top is not positioned too high or too low in the gantry (y axis of the patient). Moreover, objects at the outer periphery of the B detector may be unable to undergo optimal post-processing due to the technical specifications of the post-processing algorithm. In detail, adjacent volume elements (voxels) have to be used for calculation of the DE properties of any voxel within the field of view. Therefore, the reconstructed DE field of view will be about 5 mm smaller than the actual B detector FOV. In the periphery of the FOV, no color-coded images or virtual unenhanced images are available.

CT dose and image noise

Since the 80-kVp X-ray photons have a lower energy than a standard acquisition at 120 kVp, image noise will substantially increase in large patients. In order to minimize image noise, the mAs needs to be increased. To minimize patient exposure to ionizing radiation, abdominal dual energy CT protocols operate using an online dose modulation system (CareDOSE 4D, Siemens Medical Solutions, Forchheim, Germany) that adapts the tube current to the patient's

anatomy [3, 10]. The image quality reference mAs values are set to 400 mAs on the B tube and 96 mAs on the A tube, thereby splitting the energy between the two tubes. These settings take into account that higher mAs values on the A tube would lead to increased image noise on the B detector due to scatter radiation. On the B tube, technical limitations prevent mAs values over 600 mAs. The calculated effective patient doses for abdominal scans will range from 4.5–12.5 mSv, which is similar to the effective dose of a standard abdominal CT acquisition using 120 kVp with 250 mAs [11].

For abdominal imaging, dual energy CT acquisitions should employ a collimation of 14×1.2 mm rather than 64×0.6 mm as the latter configuration will cause increased image noise on the B detector images. Since a reconstructed slice thickness below 1.2 mm is usually not required for most applications in the abdomen, this typically does not represent a significant limitation in terms of spatial resolution. However, the data acquired are not isotropic in the X, Y, and Z dimensions.

Dual energy CT is not recommended for patients whose body mass index is >30. In morbidly obese patients, the two tubes can both be operated at 120 kVp, which will help to decrease image noise in these very large patients. The system can be used to scan patients with a body weight of up to 500 lbs (220 kg).

Image generation and post processing

Each dual energy acquisition can generate the following types of data: pure 80 kVp data, pure 140 kVp data, and a weighted average 120 kVp data set that is a composition of 70% from the A (high kV) and 30% from the B (low kV) tube. Using a slider bar, this relation can be manually adjusted on a dual energy workstation, and we found that in some patients image quality can be improved using a 50/50 ratio. In addition, using dual energy post-processing software based on the dual energy index of materials in the volume of tissue examined, virtual unenhanced CT data, an iodine data set, and a color-coded data set that shows iodine distribution over the virtual unenhanced data can be generated (Fig. 2). Regarding the applications described in this manuscript, the three materials analyzed are iodine, soft tissue, and water (virtual unenhanced and iodine distribution images), or water, calcium, and uric acid (kidney stones application). For visualization of calcifications in the setting of a contrast-enhanced examination, the algorithm will analyze iodine, calcium, and soft tissue densities.

Applications in the abdomen

Dual energy imaging of renal masses

Assessment of renal masses is based upon enhancement and conventionally requires unenhanced and contrast-enhanced CT acquisitions to be performed [12, 13]. Currently, images are acquired before the injection of iodinated contrast agent in order to allow for baseline density measurements of the renal mass and to evaluate for calcification and fat. The most important criterion for the differentiation of benign from malignant masses is the presence of enhancement in a lesion [14].

Utilizing dual energy CT, a virtual unenhanced image can be generated, and this data may be used for baseline density measurements, thereby making true unenhanced imaging unnecessary and saving radiation. This is especially useful in cases of incidentally detected renal lesions with high attenuation on enhanced CT, the main differential diagnostic considerations being hyperdense cysts and renal mass. Preliminary data show that there is good correlation between virtual unenhanced and true unenhanced CT Hounsfield units of the renal parenchyma [15]. In a study conducted at our institutions, we found mean density values of 30.8±4.0 (true unenhnanced) and 31.6±7.1 (virtual unenhanced) Hounsfield units, p=0.26.

Dual energy CT can be used for the differentiation of high-density cysts from solid renal masses (Fig. 3). Using dual energy post-processing software, the contrast agent can be digitally subtracted from the image. This can be done because the dual energy index of iodine is significantly different from the dual energy index of soft tissue and fat. The dual energy data can also be used to generate a color-coded image that shows the distribution of iodine within the volume of tissue examined by CT. This color-coded display is very sensitive to subtle enhancement. In our experience, high-density renal cysts with a density greater than the renal parenchyma (e.g., 60 HU for a hemorrhagic cyst) will be reliably identified and characterized based on measured HU values as those correlate well between unenhanced and virtual unenhanced datasets. This underlines the ability of the algorithm to deal with different high-density materials in the presence of iodine.

Off center positioning of the patient may be beneficial for imaging the kidneys if the site of the lesion is known, for example, a lesion detected on US. As stated above, the smaller field of view (FOV) of the B detector can be a limiting factor in abdominal imaging, depending on the body size of the patient. In patients with suspected or known renal masses, the patient can be shifted slightly to the contralateral side, thus ensuring that the entire kidney with the mass is included in the B detector FOV.

Dual energy imaging of urinary calculi

When evaluating the patient with flank pain and suspected urinary stones, unenhanced low-dose MDCT is the most accurate imaging technique [16, 17]. It provides the exact location of calculi within the renal parenchyma, the ureters, and the urinary bladder and can aid treatment decisions based on the size and location of the stone [18, 19]. Metabolic evaluation of patients with chronic recurrent

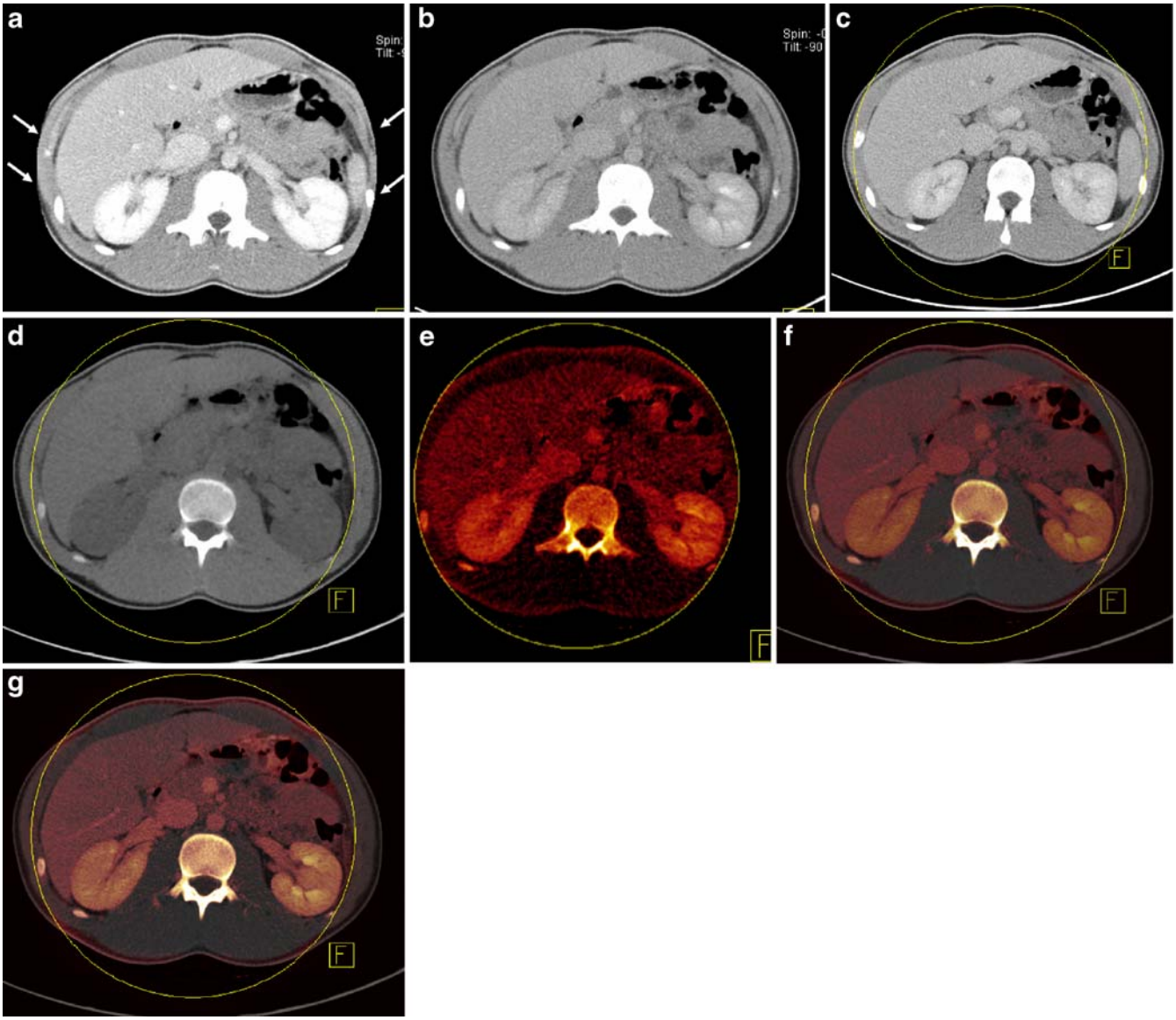

Fig. 2 Image data generated from a dual energy acquisition. **A.** Axial CT image obtained at 80 kVp and 400 mAs. In this slim patient, only the left lateral abdominal wall is not included in the 27 cm FOV (arrows). **B.** Axial CT image obtained at 140 kVp and 96 mAs. Note entire abdomen is included in the standard 50 cm FOV. **C.** Axial CT image obtained with weighted average of 80 and 140 kVp data sets. This image equals a 120 kV image from a standard CT system. The yellow line represents the B detector FOV. **D.** Virtual unenhanced image. Note slighlty increased image noise and FOV of the B detector (yellow line). **E.** Color coded iodine image showing distribution of iodine in the scan field of view (compare bright color in the kidneys). **F.** Virtual unenhanced image with color coded iodine overlay. Note simultaneous display of iodine distribution and unenhanced CT providing anatomical detail. **G.** Weighted average image with color coded iodine overlay. This image shows greater anatomical detail and information about iodine distribution

calculi is often performed in an attempt to identify an underlying metabolic abnormality [20, 21]. While MDCT can identify patients with urinary tract stones, it cannot reliably predict stone composition. The characterization of urinary stones can be important for treatment decisions. Stones consisting predominantly of uric acid can be treated with oral medication (alkalinization) rather than endoureteral extraction or extracorporeal shock wave lithotripsy (ESWL).

Studies have demonstrated that the chemical composition of calculi can be partially determined by CT in vitro, but this differentiation is less reliable in vivo [22–25]. Using dual energy CT the chemical characterization of stones is possible based on their characteristic dual energy index. Dual energy post-processing software algorithms assume a mixture of water, calcium, and uric acid for every voxel and color-code voxels that show a dual energy behavior similar to calcium in blue and one that is similar to uric acid in red (Fig. 4). Voxels that show a linear density behavior at both tube potentials remain grey. Using dual energy CT, differentiation of pure uric acid, mixed uric acid,

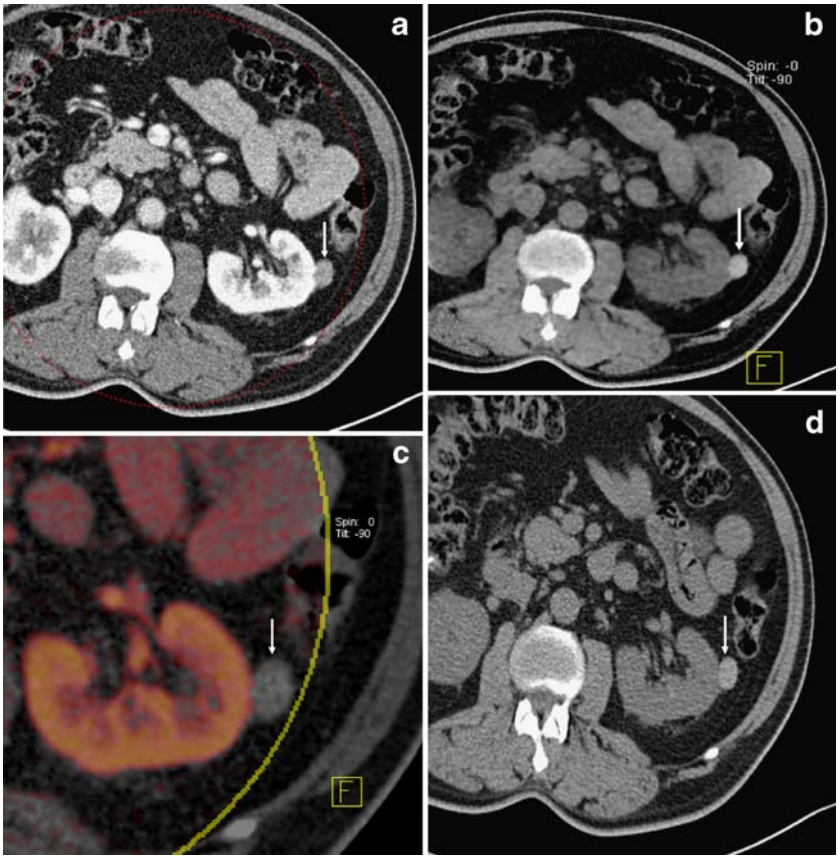

Fig. 3 DECT for characterization of renal masses. **A.** Axial contrast-enhanced CT image of the upper abdomen in a 75-year-old man. Weighted average DECT image showing a hyperdense lesion in the left kidney (arrow) measuring 75 HU. **B.** Virtual unenhanced image at the same slice position shows the lesion (arrow) has high density (70 HU). The yellow rim corresponds to the B detector field of view. Note in this large patient the periphery of the abdomen is not included in the B detector FOV (yellow circle). **C.** Color-coded DECT image showing that the lesion (arrow) does not enhance. **D.** True unenhanced image in same patient shows the lesion has high density, measuring 72 HU. This case demonstrates how a virtual unenhanced image can be used if a true unenhanced is unavailable

and calcified stones is possible [11]. Furthermore, the differentiation of struvite and cystine is possible by adapting the slope of the three-material decomposition algorithm [11].

In order to maintain a low radiation exposure, a standard unenhanced low-dose MDCT scan of the entire abdomen and pelvis using a single-source technique (tube potential, 120 kV; collimation, 64×0.6 mm; reference mAs, 40; dose modulation) can be utilized. Subsequently, a focal dual energy acquisition of the anatomical region containing the stone can be performed. Limiting the DE acquisition will substantially decrease radiation exposure. However, this approach requires the radiologist or trained technologist to evaluate the initial data set while the patient is still in the CT unit in order to determine the presence and location of stones. Based on this assessment, a localized dual energy CT examination can be planned.

Dual energy imaging of hematuria

Another potential application for dual energy CT is the evaluation of patients with hematuria. Hematuria may be caused by stone disease, renal or urothelial tumors, as well

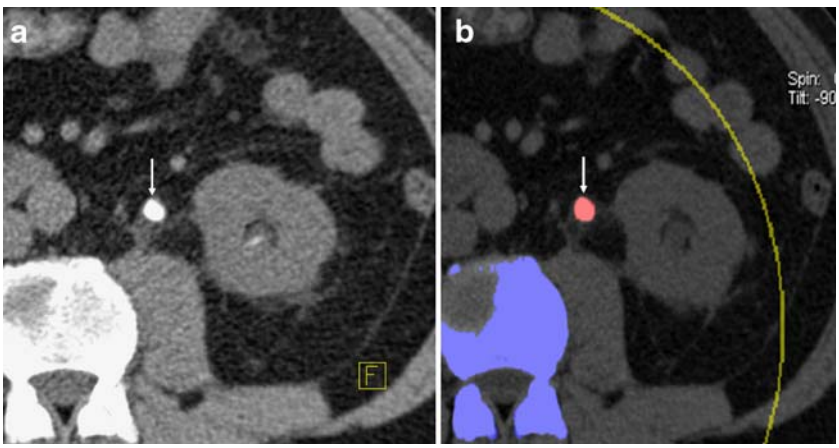

Fig. 4 DECT to differentiate urinary renal stone composition. **A.** Axial low-dose single-energy NCCT image shows an 8-mm stone in the proximal ureter in a 45-year-old male patient with acute flank pain. **B.** DECT in the same patient, same slice position. The color-coded display from the DE post processing workstation shows the composition of the stone (arrow). Red color indicates that the calculus consists of uric acid

as a variety of other inflammatory conditions of the urinary tract. There is controversy on how to best image the patient with hematuria. While there is no radiation with MR, MR imaging has a major limitation in not being able to confidently depict stones. There are numerous CT protocols for evaluating hematuria, which usually include a NCCT, a nephrographic phase (100–120 s), and a urographic phase (5–7 min post injection) [26, 27]. While these three acquisitions are important when evaluating the patient with hematuria, the acquisition imparts a large radiation does to the patient.

In order to minimize radiation exposure to the patient with hematuria, the number of acquisitions obtained after the administration of IV contrast medium can be reduced [27]. As in CT of renal masses, dual energy CT helps to reduce the number of acquisitions. If the dual energy acquisition is performed during the delayed urographic phase of enhancement, excreted contrast agent can be electronically removed from the renal pelvis and ureters, thus allowing for evaluation of the presence of urinary stones that would otherwise be obscured by the dense contrast material (Fig. 5) [25]. Therefore, a true unenhanced acquisition may be eliminated. Moreover, if a split bolus technique is used, a single contrast-enhanced acquisition yielding both dual energy nephrographic including virtual unenhanced and urographic data may be potentially all that is required to evaluate the patient with hematuria.

Dual energy CT after abdominal aortic aneurysm repair

Traditionally, patients who undergo endovascular repair of abdominal aortic aneurysms (AAA) are evaluated using a multi-phase CT protocol [28]. Unenhanced, arterial and venous phase acquisitions have been utilized for optimization of the detection of possible complications including endoleaks [29]. The possibility to eliminate the arterial phase without loss of diagnostic information with a dose savings of up to 36.5% of the total radiation has been shown to be feasible [30]. Using this protocol an unenhanced and 60-s examination are acquired. The true unenhanced phase typically cannot be omitted because it demonstrates calcifying thrombus in the lumen of the aneurysm. Without the unenhanced acquisition, differentiation of calcifying thrombus from an endoleak may be difficult or impossible. The typical appearance of an endoleak is a blush of contrast agent in the aneurysm sac. Dual energy CT can provide information about high density material within the thrombosed lumen of the aneurysm by generating a virtual unenhanced data set and can therefore potentially eliminate the true unenhanced acquisition. This can substantially reduce radiation exposure (Fig. 6). In addition, since the attenuation of iodine is greater at 80 kVp than at 120/140 kVp, the possibility that small endoleaks will be seen more easily at 80 kVp exists.

Dual energy CT of adrenal adenomas

In up to 5% of patients undergoing contrast-enhanced abdominal CT, an incidental adrenal mass is discovered [31]. In order to differentiate a lipid-rich adrenal adenoma from pheochromocytomas and other masses such as metastases, patients have to either undergo additional unenhanced CT or chemical shift MR imaging [32]. The diagnostic criterion at unenhanced CT that is used to make the diagnosis of adrenal adenoma is low mean attenuation of the lesion <10–15 HU, which is caused by the presence of intracellular fat [32]. In cases with higher attenuation, MRI utilizing in- and opposed-phase imaging may be helpful in confirming the diagnosis of adenoma since it appears to be somewhat more sensitive to the presence of intracytoplasmic fat [33]. However, by acquiring abdominal CT with a dual energy acquisition, virtual unenhanced data sets can be generated. If an adrenal mass is inicdentally detected during contrast-enhanced CT of the abdomen, these data can be used to determine its density (Fig. 7). Currently, all patients who undergo adnominal CT on the dual energy unit at our institution have routine

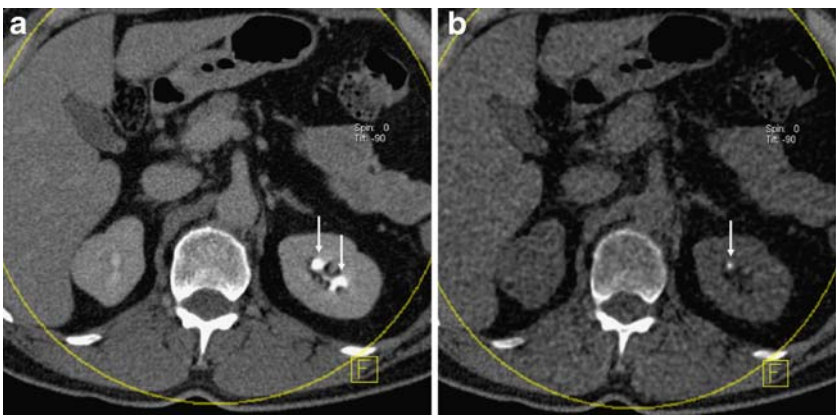

Fig. 5 DECT for the evaluation of hematuria. **A.** Axial weighted average DECT image in the urographic phase shows contrast agent in the left renal collecting system (arrows) in a 63-year-old male imaged for evaluation of hematuria. **B.** In the same patient, virtual unenhanced image at the same slice position identifies a 4-mm stone in the anterior left collecting system (arrow). The stone only becomes visible after subtraction of iodine from the image

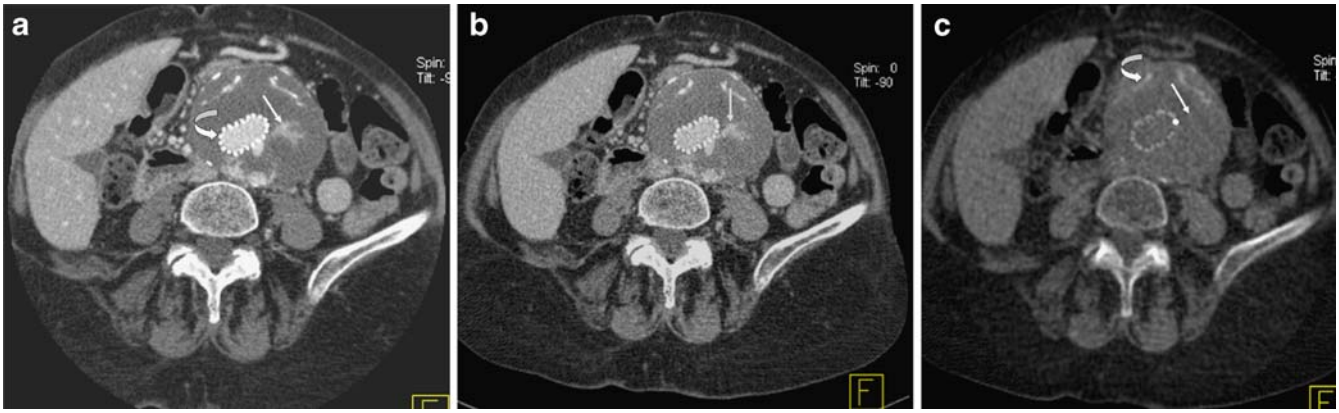

Fig. 6 DECT in status post-endovascular repair of AAA. **A.** On the 80-kV image, a type 2 endoleak (arrow) is identified in a 72-year-old male. The density of the contrast agent in the aneurysm sac is 320 HU. Note stent graft (curved arrow). **B.** Weighted average DECT image at the same slice position. The endoleak (arrow) is less conspicuous, measuring 220 HU. **C.** Virtual unenhanced DECT image at the same slice position. Iodine has been subtracted, confirming the endoleak (arrow). Note calcified thrombus in the aneurysm sac (curved arrow)

virtual unenhanced data sets sent to the PACS. This enables an assessment of both adrenal and renal masses incidentally discovered at CT.

Dual energy CT of pancreatic tumors

Pancreatic adenocarcinoma typically appears as a hypodense mass at CT. The low attenuation is primarily due to fibrosis and desmoplasia within the tumor. Dual-phase imaging of the pancreas performed during the pancreatic phase (approximately 40 s) and portal venous phases of enhancement at CT optimizes detection of pancreatic neoplasms [33]. The tumor usually appears more conspicuous during the pancreatic as opposed to the venous phase of enhancement because of the fibrosis and desmoplasia within the tumor.

In the setting of pancreatic adenocarcinoma, MDCT allows depiction of the tumor, visualization of the peripancreatic vessels, lymph nodes, and distant metastases, allowing for high accuracy in staging [34]. However, occasionally it may be difficult to detect pancreatic adenocarcinoma even utilizing dual-phase imaging. One study showed that in up to 11% of cases, pancreatic adenocarcinoma is iso-attenuating to the surrounding parenchyma on both the pancreatic and the venous phases of the acquisition [33]. Another study demonstrated that upon retrospective review, patients with proven pancreatic adenocarcinoma who had undergone prior CT had subtle findings at the initial CT that suggested the diagnosis [35]. In most cases the neoplasm was not seen, but a dilated pancreatic duct was present.

Since the normal pancreas enhances vividly during the pancreatic phase and contains much more iodine than a

Fig. 7 DECT for adrenal mass characterization. **A.** Axial weighted average DECT image in a 68-year-old man shows a 2.1-cm solid mass (arrow) in the left adrenal gland. The density of the mass is 45 HU. **B.** Virtual unenhanced image at the same slice position shows the mass is hypoattenuating measuring 5 HU (arrow). This is most consistent with an andrenal adenoma. **C.** The true unenhanced image at the same slice position confirms the low density of the mass (arrow), measuring 5 HU

pancreatic adenocarcinoma, dual energy CT may improve detection and allow a more accurate assessment of the size of the tumor compared with non-dual energy acquisitions. We have noted that pancreatic adenocarcinoma may be more conspicuous when viewed with low (80) kVp data sets than at 120 or 140 kVp (Fig. 8). This is related to the differences in the amount of iodine within these different tissues. These characteristics may prove to be helpful in the detection of tumors that show enhancement patterns similar to the normal parenchyma of the gland. The potential for dose reduction is also possible. Two separate acquisitions may no longer be needed if indeed tumor conspicuity is maintained during the portal venous phase of imaging when viewed at 80 kVp, thus potentially eliminating the need for the pancreatic phase of enhancement.

Dual energy CT of the liver

MDCT of the liver allows reliable detection and differentiation of hepatic abnormalities like cysts, hemangiomas, metastases, or hepatocellular and cholangiocellular carcinomas [36, 37]. For detection and characteriazation of hepatic masses, intravenous injection of contrast agent is mandatory, and in many instances multi-phasic imaging will be performed. Unenhanced images will be acquired in patients with calcified masses or status post chemoembolization for visualization of lipiodol particles within treated lesions [38]. Like in renal dual energy CT, true unenhanced images can be replaced with virtual unenhanced images in hepatic dual energy CT. Color-coded iodine images show the distribution of iodine. DECT may be used for sensitive detection of subtle contrast enhancement in hypodense liver lesions (see Fig. 9), thereby enabling rapid differentiation of malignant masses from cysts. Another application in the liver concerns treatment monitoring. Increasingly, patients with colorectal or breast cancer metastases to the liver are being treated with either antiangiogenic drugs, radiofrequency ablation, or SIRT (selective internal radiotherapy) using Yttrium-90 microspheres. These treatments often lead to altered perfusion and iodine uptake of liver lesions. This can be visualized using dual energy CT. Preliminary results from our institution show that decreased iodine uptake quantified at DECT is an independent predictor of response to antiangiogenic treatment in patients with metastasized GIST (gastrointestinal stroma tumor). Figure 9 shows differentiation of metastasis from a simple cyst on contrast-enhanced dual energy CT of the liver.

Dual energy CT of the small bowel

CT enterography is performed with neutral oral contrast medium and a rapid bolus of IV contrast medium to facilitate imaging of the small bowel. It is utilized to visualize various pathological conditions affecting the small bowel, including obscure GI bleeding, Crohn's disease, and various inflammatory and ischemic conditions [39]. Neutral oral contrast agents are used to distend the small bowel. After the administration of a rapid bolus of IV contrast medium, the degree of enhancement and enhancement pattern is easily seen [39, 40]. In the setting of Crohn's disease, increased enhancement of the bowel wall has been shown to correlate with the histological degree of inflammation [41]. On standard CT images acquired at

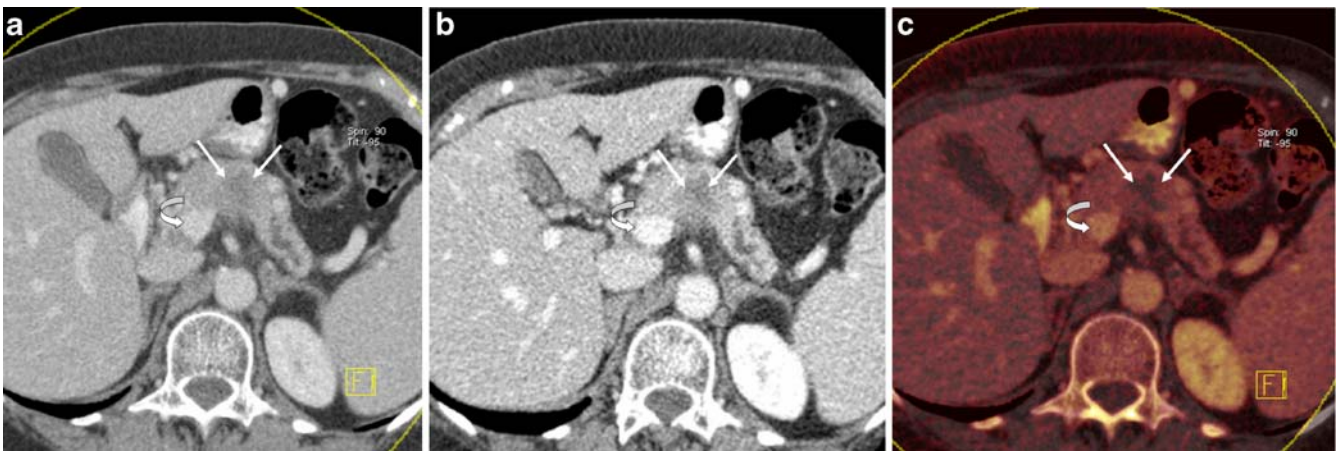

Fig. 8 DECT in imaging of pancreatic masses. **A.** Weighted average axial DECT image in a 72-year-old female patient shows marked dilatation of the pancreatic duct due to a 2.5-cm hypoattenuating mass (arrow). The mass measures 60 HU, and the surrounding normal pancreatic parenchyma 89 HU. Note SMV (curved arrow). **B.** An 80-kV image from DECT at same slice position shows greater consicuity of the mass (arrows) that measures 81 HU, while the density of the surrounding pancreas is 155 HU. Note increased density of SMV (curved arrow). **C.** Color-coded DECT image at same slice position shows excellent delineation of the mass (arrows) and provides information on reduced iodine uptake. SMV (curved arrow)

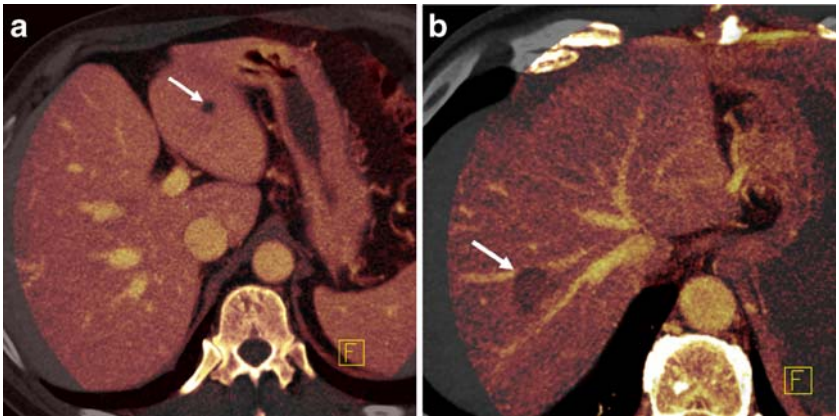

Fig. 9 DECT imaging of liver lesions. **A.** Axial color-coded DECT image showing simple cyst in the left lobe of the liver. There is no enhancement in the mass. **B.** Axial color-coded DECT image showing an enhancing mass in the right hepatic lobe in a patient with GIST. Cleary, enhancement is seen within the mass

120 kVp, it can be difficult to discriminate between physiological and abnormal enhancement of the small bowel wall. Since low kVp images display greater density of contrast agent than standard images, dual energy CT might help to determine the presence of subtle inflammation when data are viewed at 80 kVp (Fig. 10). Similarly, in patients with suspected small bowel ischemia differences in enhancement between poorly perfused ischemic small bowel and adjacent normal segments may be accentuated.

Limitations

Despite the numerous clinical opportunities that dual source dual energy CT allows, several important limitations exist. As previously stated, the "B" tube has a smaller field of view than the standard field of view with the "A" tube. Moreover, the very peripheral part of the FOV of the B tube cannot be utilized for dual energy post-processing. Therefore, in large/wide patients, the periphery of the patient will not be included in the field. While this does not affect the overall image quality of the exam, it does affect the ability to exploit the benefits of dual energy in these regions.

This FOV limitation will not be a problem for the aorta, pancreas, adrenal glands, or small bowel. However, it may be problematic for some renal masses. As stated above, if a known renal mass is to be imaged, the patient can be positioned eccentrically to take advantage of the dual energy capabilities.

Data sets of 80 kVp inherently have more noise than images acquired at 120 or 140 kVp. As a result, dual energy acquisitions are ineffective in obese patients or patients with very large abdomens. Also related to the noise in the scan, data should not be acquired with the thinnest detector configuration. On the current scanner a detector configuration of 1.2 mm is used as opposed to 0.6 mm. For most abdominal applications, this is not a severe limitation as data can be reconstructed at 1.2-mm thickness, allowing reasonable Z-axis resolution for multiplanar reformatting and volume rendering.

Finally, one could assume that the radiation dose to the patient theoretically could be increased using a dual energy acquisition. However, utilizing the protocols discussed earlier in this review, a typical dual energy CT scan of the abdomen results in an effective dose similar to a routine standard CT of the abdomen performed without a dual energy technique. Moreover, the potential to decrease the overall radiation exposure to patients by eliminating the routine acquisition of unenhanced data is a major benefit of dual energy CT.

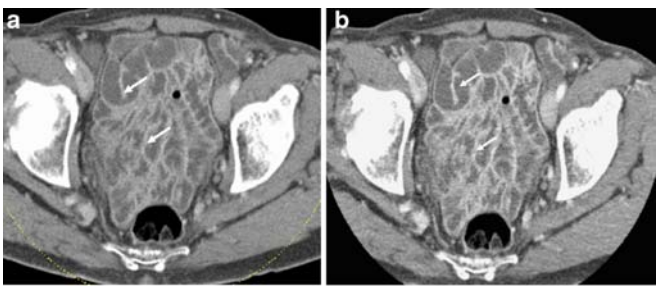

Fig. 10 DECT in imaging of the small bowel. **A.** Axial weighted average DECT image in 78-year-old man shows normal small bowel mucosa (arrows) of the jejunum. **B.** An 80-kV image at same slice position shows marked increase in attenuation of the mucosa (arrows) of the small bowel

Conclusion

Dual energy CT has several potential applications in abdominal imaging. First virtual NCCT data sets are useful in many ways. They can be used to assess for hepatic steatosis, determine baseline density measurements in renal and adrenal masses, and differentiate calcium and iodine in patients status post-AAA repair. Using dual energy CT,

determining the composition of various kidney stones is possible, thus aiding in treatment decisions. Low kVp images from the B detector provide increased conspicuity of hypoattenuating masses in the pancreas, and color-coded images may aid in the detection of small tumors. Moreover, if tumor conspicuity is maintained at portal venous phase imaging, the pancreatic phase may be eliminated, thus reducing radiation exposure to patients. In addition, the low 80-kVp images may aid in visual assessment of small bowel enhancement and hence perfusion.

For all clinical applications, collimation should be 14× 1.2 mm in order to avoid excess image noise. Careful patient positioning will greatly improve image quality and help to overcome technical limitations. Continued research with dual energy CT will help to determine the optimal utilization and indications of this new technology.

References

1. Hounsfield GN (1995) Computerized transverse axial scanning (tomography): Part I. Description of system, 1973. Br J Radiol 68:H166–H172
2. Flohr TG, McCollough CH, Bruder H et al (2006) First performance evaluation of a dual-source CT (DSCT) system. Eur Radiol 16:256–268
3. Johnson TR, Krauss B, Sedlmair M et al (2007) Material differentiation by dual energy CT: initial experience. Eur Radiol 17:1510–1517
4. Kalva SP, Sahani DV, Hahn PF et al (2006) Using the K-edge to improve contrast conspicuity and to lower radiation dose with a 16-MDCT: a phantom and human study. J Comput Assist Tomogr 30:391–397
5. Genant HK, Boyd D (1977) Quantitative bone mineral analysis using dual energy computed tomography. Invest Radiol 12:545–551
6. Goldberg HI, Cann CE, Moss AA et al (1982) Noninvasive quantitation of liver iron in dogs with hemochromatosis using dual-energy CT scanning. Invest Radiol 17:375–380
7. Cann CE, Gamsu G, Birnberg FA et al (1982) Quantification of calcium in solitary pulmonary nodules using single- and dual-energy CT. Radiology 145:493–496
8. Chiro GD, Brooks RA, Kessler RM et al (1979) Tissue signatures with dual-energy computed tomography. Radiology 131:521–523
9. Johnson TR, Nikolaou K, Wintersperger BJ et al (2006) Dual-source CT cardiac imaging: initial experience. Eur Radiol 16:1409–1415
10. Graser A, Wintersperger BJ, Suess C et al (2006) Dose reduction and image quality in MDCT colonography using tube current modulation. AJR Am.J. Roentgenol 187:695–701
11. Graser A, Johnson TR, Bader M et al (2008) Dual energy CT characterization of urinary calculi: Initial in vitro and clinical experience. Invest Radiol 43:112–119
12. Szolar DH, Kammerhuber F, Altziebler S et al (1997) Multiphasic helical CT of the kidney: increased conspicuity for detection and characterization of small (<3-cm) renal masses. Radiology 202:211–217
13. Birnbaum BA, Jacobs JE, Ramchandani P (1996) Multiphasic renal CT: comparison of renal mass enhancement during the corticomedullary and nephrographic phases. Radiology 200:753–758
14. Israel GM, Bosniak MA (2005) How I do it: Evaluating renal masses. Radiology 236:441–450
15. Graser A (2007) Dual energy CT in the assessment of renal masses: Can dual energy virtually unenhanced images replace noncontrast scanning? RSNA 2007 Chicago, IL, USA
16. Boulay I, Holtz P, Foley WD et al (1999) Ureteral calculi: diagnostic efficacy of helical CT and implications for treatment of patients. AJR Am J Roentgenol 172:1485–1490
17. Smith RC, Rosenfield AT, Choe KA et al (1995) Acute flank pain: comparison of non-contrast-enhanced CT and intravenous urography. Radiology 194:789–794
18. Poletti PA, Platon A, Rutschmann OT et al (2007) Low-dose versus standard-dose CT protocol in patients with clinically suspected renal colic. AJR Am J Roentgenol 188:927–933
19. Kluner C, Hein PA, Gralla O et al (2006) Does ultra-low-dose CT with a radiation dose equivalent to that of KUB suffice to detect renal and ureteral calculi? J Comput Assist Tomogr 30:44–50
20. Park S (2007) Medical management of urinary stone disease. Expert Opin Pharmacother 8:1117–1125
21. Moe OW (2006) Kidney stones: pathophysiology and medical management. Lancet 367:333–344
22. Hillman BJ, Drach GW, Tracey P et al (1984) Computed tomographic analysis of renal calculi. AJR Am J Roentgenol 142:549–552
23. Mostafavi MR, Ernst RD, Saltzman B (1998) Accurate determination of chemical composition of urinary calculi by spiral computerized tomography. J Urol 159:673–675
24. Nakada SY, Hoff DG, Attai S et al (2000) Determination of stone composition by noncontrast spiral computed tomography in the clinical setting. Urology 55:816–819
25. Alkadhi H and al. e (2007) Dual-energy contrast-enhanced computed tomography for the detection of urinary stone disease. Invest Radiol 42:
26. Van Der Molen AJ, Cowan NC, Mueller-Lisse UG et al (2008) CT urography: definition, indications and techniques. A guideline for clinical practice Split-bolus MDCT urography with synchronous nephrographic and excretory phase enhancement. Eur Radiol Eur Radiol 18:4–17 Epub 2007 Nov 1
27. Chow LC, Kwan SW, Olcott EW et al (2007) Split-bolus MDCT urography with synchronous nephrographic and excretory phase enhancement. AJR Am J Roentgenol AJR Am J Roentgenol 189:314–322
28. Mita T, Arita T, Matsunaga N et al (2000) Complications of endovascular repair for thoracic and abdominal aortic aneurysm: an imaging spectrum. Radiographics 20:1263–1278
29. Rozenblit AM, Patlas M, Rosenbaum AT et al (2003) Detection of endoleaks after endovascular repair of abdominal aortic aneurysm: value of unenhanced and delayed helical CT acquisitions. Radiology 227:426–433
30. Macari M, Chandarana H, Schmidt B et al (2006) Abdominal aortic aneurysm: can the arterial phase at CT evaluation after endovascular repair be eliminated to reduce radiation dose? Radiology 241:908–914
31. Korobkin M, Francis IR, Kloos RT et al (1996) The incidental adrenal mass. Radiol.Clin North Am 34:1037–1054

32. Israel GM, Korobkin M, Wang C et al (2004) Comparison of unenhanced CT and chemical shift MRI in evaluating lipid-rich adrenal adenomas. AJR Am J Roentgenol 183:215–219
33. Prokesch RW, Chow LC, Beaulieu CF et al (2002) Isoattenuating pancreatic adenocarcinoma at multi-detector row CT: secondary signs. Radiology 224:764–768
34. Prokesch RW, Chow LC, Beaulieu CF et al (2002) Local staging of pancreatic carcinoma with multi-detector row CT: use of curved planar reformations initial experience. Radiology 225:759–765
35. Gangi S, Fletcher JG, Nathan MA et al (2004) Time interval between abnormalities seen on CT and the clinical diagnosis of pancreatic cancer: retrospective review of CT scans obtained before diagnosis. AJR Am J Roentgenol 182:897–903
36. Semelka RC, Martin DR, Balci C et al (2001) Focal liver lesions: comparison of dual-phase CT and multisequence multiplanar MR imaging including dynamic gadolinium enhancement. J Magn Reson Imaging 13:397–401
37. Kamel IR, Choti MA, Horton KM et al (2003) Surgically staged focal liver lesions: accuracy and reproducibility of dual-phase helical CT for detection and characterization Focal liver lesions: comparison of dual-phase CT and multisequence multiplanar MR imaging including dynamic gadolinium enhancement. Radiology 227:752–757
38. Schima W, Ba-Ssalamah A, Kurtaran A et al (2007) Post-treatment imaging of liver tumours. Cancer Imaging 7(Spec No A):S28–S36
39. Macari M, Megibow AJ, Balthazar EJ (2007) A pattern approach to the abnormal small bowel: observations at MDCT and CT enterography. AJR Am J Roentgenol 188:1344–1355
40. Megibow AJ, Babb JS, Hecht EM et al (2006) Evaluation of bowel distention and bowel wall appearance by using neutral oral contrast agent for multi-detector row CT. Radiology 238:87–95
41. Bodily KD, Fletcher JG, Solem CA et al (2006) Crohn Disease: mural attenuation and thickness at contrast-enhanced CT Enterography–correlation with endoscopic and histologic findings of inflammation. Radiology 238:505–516